JACS
JOURNAL OF THE AMERICAN CHEMICAL SOCIETY
Article
pubs.acs.org/JACS

Ultrafast Charge Transfer and Hybrid Exciton Formation in 2D/0D Heterostructures

Abdelaziz Boulesbaa,* Kai Wang, Masoud Mahjouri-Samani, Mengkun Tian, Alexander A. Puretzky, Ilia Ivanov, Christopher M. Rouleau, Kai Xiao, Bobby G. Sumpter, and David B. Geohegan

Center for Nanophase Materials Sciences, Oak Ridge National Laboratory, Oak Ridge, Tennessee 37831, United States

Supporting Information

ABSTRACT: Photoinduced interfacial charge transfer is at the heart of many applications, including photovoltaics, photocatalysis, and photodetection. With the emergence of a new class of semiconductors, i.e., monolayer two-dimensional transition metal dichalcogenides (2D-TMDs), charge transfer at the 2D/2D heterojunctions has attracted several efforts due to the remarkable optical and electrical properties of 2D-TMDs. Unfortunately, in 2D/2D heterojunctions, for a given combination of two materials, the relative energy band alignment and the charge-transfer efficiency are locked. Due to their large variety and broad size tunability, semiconductor quantum dots (0D-QDs) interfaced with 2D-TMDs may become an attractive heterostructure for optoelectronic applications. Here, we incorporate femtosecond pump−probe spectroscopy to reveal the sub-45 fs charge transfer at a 2D/0D heterostructure composed of tungsten disulfide monolayers (2D-WS_2) and a single layer of cadmium selenide/zinc sulfide core/shell 0D-QDs. Furthermore, ultrafast dynamics and steady-state measurements suggested that, following electron transfer from the 2D to the 0D, hybrid excitons, wherein the electron resides in the 0D and the hole resides in the 2D-TMD monolayer, are formed with a binding energy on the order of ∼140 meV, which is several times lower than that of tightly bound excitons in 2D-TMDs.

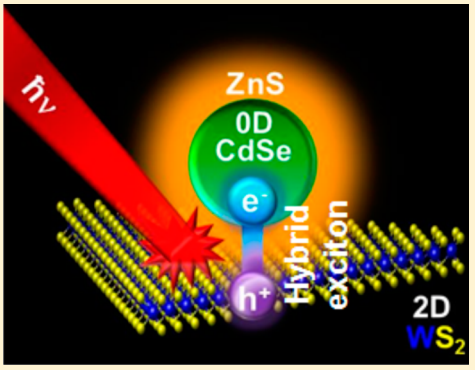

INTRODUCTION

Unlike graphene, two-dimensional transition metal dichalcogenides (2D-TMDs) are semiconductors with a direct bandgap.[1−4] Despite their atomic thickness, they strongly absorb light,[1] which makes them ideal platforms for photovoltaic and photodetector devices.[1,5,6] Because charge carriers in these semiconductors are confined within a 2D plane of the material,[7] Coulomb interactions are greatly enhanced which opens up new electric and dielectric screening phenomena.[8] Another class of nanomaterials with remarkable optical properties is colloidal semiconducting quantum dots (0D-QD), which exhibit high absorption cross-sections, broad tunability of bandgaps and high quantum efficiencies.[9] Combining these two nanomaterial classes into one hybrid nanostructure may bring additional capabilities and open new opportunities for optoelectronic applications. Indeed, the hybrid 2D/0D interface has already attracted several research efforts.[10−12] In a nanocomposite of cadmium selenide/cadmium zinc sulfide (CdSe/CdZnS core/shell) 0D-QDs and 2D-MoS_2, the efficiency of non-radiative Förster resonant energy transfer (FRET) from the 0D to the 2D material increased as the number of MoS_2 layers decreased, reaching 95% in the case of a monolayer.[10] In a similar system (CdSSe/MoS_2), FRET efficiency was modulated up to 500% by a gate-induced variation in the excitonic absorption of the 2D-MoS_2, thereby allowing selective tuning of the 0D-QDs photoluminescence (PL) toward new spectral bands.[11]

For heterojunctions between different 2D metal dichalcogenides (e.g., MoS_2, WS_2, $MoSe_2$, WSe_2), interfacial charge exchange has been observed on a sub-picosecond time-scale.[13−17] For example, in the type II semiconductor heterojunction between WS_2 and MoS_2, hole transfer from MoS_2 to WS_2 was reported to take place within 50 fs after excitation.[13] In addition, at a MoS_2/$MoSe_2$ interface, both electron transfer from $MoSe_2$ to MoS_2 and hole transfer in the opposite direction were reported to occur on a ps time-scale.[14] Due to type II semiconductor band energy alignment in these 2D/2D interfaces, charge transfer led to the formation of an indirect exciton (IX), where the electron is located in the conduction band (CB) of one 2D material and the hole in the valence band (VB) of the other 2D material.[13,14] As evidence of IX formation, some of these efforts have reported IX PL;[15−17] however, a direct measurement of IX absorption has not yet been achieved.[18]

An interesting question arises if one considers a 2D/0D hybrid interface composed of a 0D-QD structure and a 2D-TMD monolayer that has type II semiconductor band energy alignment favoring charge exchange: Will indirect excitons form in such hybrid systems? If so, the IX would have one charge in the 0D-QD and the other in the 2D-TMD, effectively forming a hybrid indirect exciton (HX). Due to the size adjustability and

Received: August 24, 2016
Published: October 18, 2016

DOI: 10.1021/jacs.6b08883
J. Am. Chem. Soc. 2016, 138, 14713−14719

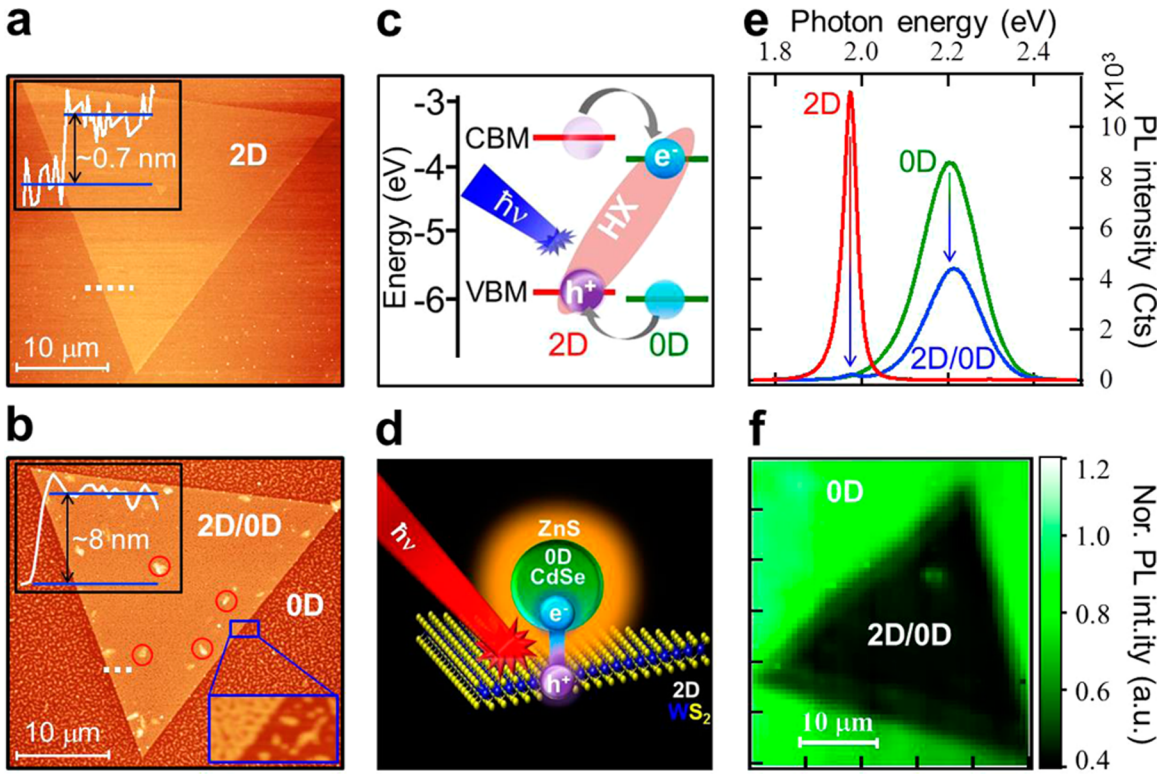

Figure 1. 2D-WS_2/0D-QDs hybrid nano-interface. (a) AFM image of an as-synthesized 2D-WS_2 crystal without 0D-QDs. The height profile measured along the dotted line is shown in the inset. The height of the 2D-WS_2 crystal is ∼7 Å, which is typical for a WS_2 monolayer. (b) AFM image of the same 2D-WS_2 crystal shown in (a) but after spin coating of CdSe/ZnS 0D-QDs. The bottom right inset shows a magnified portion of the edge as indicated, and the top left inset shows the height profile measured along the dotted line. Red circles indicate 0D-QDs aggregates. (c) Band energy alignment of the 0D and the 2D structures, with the VBM and CBM values for the non-interacting 0D-QDs and the 2D-WS_2 semiconductor taken from previous reports, refs 21 and 22, respectively. Following photoexcitation and electron transfer from the 2D to the 0D and/or hole transfer in the opposite direction, the HX is formed between the electron at the 0D CB edge and the hole at the 2D VB edge. (d) Schematic representation of HX formation upon photoexcitation. (e) PL spectra of 2D-WS_2, 0D-QD and 2D/0D heterostructure on SiO_2/Si substrate upon excitation at 3.1 eV. (f) PL map of a 2D-WS_2 crystal covered with 0D-QDs (the emission of 0D-QDs at ∼2.25 eV was monitored), showing that the 0D-QDs emission is bright (green) outside the 2D-WS_2 crystal and quenched at the heterostructure (dark triangle).

availability of QDs, the flexibility to tune the CB offset of 0D-QDs with 2D-TMD semiconductors makes them extremely attractive to tailor novel 2D/0D heterostructures for various applications, such as photovoltaics and photodetectors. In this work, we incorporate steady-state and ultrafast spectroscopy techniques to investigate HX formation and characterize ultrafast electron transfer from 2D-WS_2 monolayers to a single layer of CdSe/ZnS core/shell 0D-QDs. Femtosecond pump−probe measurements indicate that upon photoexcitation of the 2D-WS_2 monolayer, electron transfer to the 0D-QD takes place within the laser pulse duration (∼45 fs). As a result, the transferred electrons located at the QD CB bind to the holes left in the 2D VB, forming HXs. This interfacial charge exchange within the 2D/0D heterostructures may open new opportunities for optoelectronic applications of 2D and 0D nanomaterials.

RESULTS AND DISCUSSION

2D-WS_2 monolayers were prepared using chemical vapor deposition (CVD) as reported previously.[19] To form the 2D/0D hybrid interface, core/shell CdSe/ZnS QDs with octadecylamine capping ligand (Ocean NanoTech) were dispersed onto the 2D-WS_2 sample using spin-coating (3000 rpm) of a dilute solution of 0D-QDs in toluene (2.5 mg/mL). In order to characterize the morphology of 0D-QDs and the 2D/0D nanocomposite, transmission electron microscopy (TEM) and atomic force microscopy (AFM) measurements were carried out. High-resolution TEM images shown in Figure S1 in the Supporting Information indicate that the core/shell 0D-QD have, on average, 8.1 nm size and are spaced by ∼2 nm, which corresponds to the octadecylamine capping ligand. Taking into consideration that the thickness of the ZnS shell is ∼2 nm,[20] one can estimate the size of the CdSe core to be ∼4 nm, having its lowest exciton 1S at ∼2.25 eV.[21] Shown in Figure 1a,b are AFM images and height profiles of a 2D-WS_2 crystal before and after the 0D-QD particles were loaded on it, respectively. The height profile of the 2D-WS_2 crystal is ∼0.7 nm, which is typical for a WS_2 monolayer,[19] and the height of CdSe/ZnS 0D-QDs was further confirmed in the AFM image shown in Figure 1b to be on the order of ∼8 nm. Furthermore, this AFM image shown in Figure 1b indicates a homogeneous coverage of the sample by 0D-QDs, with the exception of few bright spots (inside red circles), which reflect local aggregates.

The size of CdSe core of the 0D-QDs was chosen in such a way as to have the band energy alignment of the 2D/0D nanocomposite allowing electron transfer from the 2D-WS_2 to the 0D-QDs and/or hole transfer in the opposite direction, as shown in Figure 1c. The valence band maximum and conduction band minimum (VBM and CBM, respectively) values for the non-interacting 0D-QDs and the 2D-WS_2 semiconductor are taken from previous reports, refs 21 and 22, respectively. Based on these values, the differences between

DOI: 10.1021/jacs.6b08883
J. Am. Chem. Soc. 2016, 138, 14713−14719

CBMs and VBMs are ~300 and ~100 meV, respectively, indicating that the driving force for electron transfer from the 2D-WS_2 monolayer to 0D-QDs is greater than that for hole transfer in the opposite direction.

A schematic of the HX formation at the 2D/0D interface upon photoexcitation is shown in Figure 1c,d. Specifically, following excitation with photons having sufficient energy for exciton generation in the 0D-QDs and 2D-WS_2 structures, an HX can be formed as a consequence of hole transfer from the 0D-QDs to the 2D-WS_2 material or through electron transfer in the opposite direction. Noting that energy transfer from the 0D-QDs to the 2D-WS_2 material is a possible pathway. In order to reveal which charge or energy exchange pathway takes place at this hybrid interface, steady-state PL spectroscopy was employed. Shown in Figure 1e are PL spectra obtained from 2D-WS_2, 0D-QDs, and the combination thereof, all on a Si/SiO_2 substrate with photoexcitation at 3.1 eV. In the case of 2D/0D nanocomposite, both emissions of the 0D-QD and the 2D-WS_2 are quenched. According to the PL map of the 2D-WS_2/0D-QD sample shown in Figure 1f, where the 0D-QDs emission was monitored around 2.25 eV (0D-QDs PL peak), the QDs emission outside the 2D-WS_2 crystal was high (green color) but on the 2D-WS_2 crystal it is quenched (dark triangle). First we note that some decrease in the 2D-WS_2 PL intensity in the presence of 0D-QDs may be due to absorption and scattering by the 0D-QD layer of the incident and emitted photons. Although, quantifying the losses due to scattering is challenging, the effect of absorption by the 0D-QD single layer can be estimated based on the absorption spectrum of the 0D-QDs. At the excitation photon energy (3.1 eV), the 0D-QDs absorb about 7% of the incident photons, and at the 2D-WS_2 PL photon energy (~2 eV), the 0D-QDs have negligible absorption. Based on Figure 1e, the 2D-WS_2 PL was quenched by ~98% (estimated by comparing the area under the PL peaks). Therefore, the absorption by the 0D-QD single layer can be responsible only for ~7% of the PL quenching, but not for the remaining ~90% of this effect. The 90% PL quenching factor was used to estimate the time-scale of charge transfer (see Supporting Information) similar to a previous report for the $MoSe_2$/WS_2 heterostructure.[23]

Since in these PL measurements the photoexcitation at 3.1 eV leads to the generation of excitons in both structures, the quenching of PL in both structures can result from energy and/or charge transfers at the interface. Based on the band energy alignment shown in Figure 1d, the pathway of energy transfer from the 2D-WS_2 to the 0D-QD material is excluded due to the 2D-WS_2 material having a smaller bandgap. This is confirmed by the fact that the 0D-QD emission was quenched—i.e., if there *was* energy transfer from the 2D-WS_2 to the 0D-QD material, one would expect an *enhancement* in the 0D-QD PL. In terms of energy transfer in the other direction—i.e., from the 0D-QD to the 2D-WS_2 material—this *is* possible, but one would expect an *enhancement* of the 2D-WS_2 PL. However, according to Figure 1e, the 2D-WS_2 emission was quenched by more than 90%, and consequently this channel of energy transfer can be ruled out.

Electron Transfer versus Hole Transfer. To investigate which charge-transfer pathway was responsible for the quenching of emission in both structures, we carried out a PL lifetime control experiment. More specifically, in addition to the ~4 nm CdSe core diameter QDs, we studied ~6.5 nm CdSe core diameter QDs which emit at 1.9 eV (see Figure 2). Since the effective mass of the hole in the VB in 0D-QDs is more than 3 times that of the electron in the CB,[24,25] the position of the 0D-QD VBM with respect to the vacuum level is essentially insensitive to the size of the 0D-QD (see Figure 2a).[21] Thus, upon interfacing these two 0D-QDs with the 2D-WS_2 monolayer, the *hole*-transfer driving forces are *similar*, while that for electron transfer from the 2D-WS_2 monolayer to the 0D-QD increases for the 6.5 nm CdSe core diameter 0D-QD. If hole transfer from the 0D-QD to the 2D-WS_2 was the channel responsible for PL quenching observed in Figure 1e, one would expect the 0D-QD lifetime decay in the presence of the 2D-WS_2 monolayer for both sizes to be similar. But, according to the measurements shown in Figure 2b, the PL decay in the case of the 6.5 nm CdSe core diameter 0D-QD was faster. This indicates that hole transfer from the 0D-QD to the 2D-WS_2 crystal is not the dominant charge-transfer process responsible for the PL quenching shown in Figure 1e,f. Furthermore, since the band gap of the 6.5 nm CdSe core diameter 0D-QD is 1.9 eV, which is smaller than that of the 2D-WS_2 crystal (~2 eV), and the fact that the PL decay was even more efficient for this size compared to the case of the 4 nm 0D-QD, it confirms that energy transfer from the 0D-QDs to the 2D-WS_2 crystal is not the process responsible for the PL quenching shown in Figure 1e,f. In conclusion, the fact that the 0D-QD's PL decay was more efficient in the case of the 6.5 nm CdSe core diameter 0D-QD, where the electron-transfer driving force is greater, indicates that electron transfer from the 2D-WS_2 crystal to 0D-QDs is the dominant process responsible for the PL quenching observed in Figures 1e.

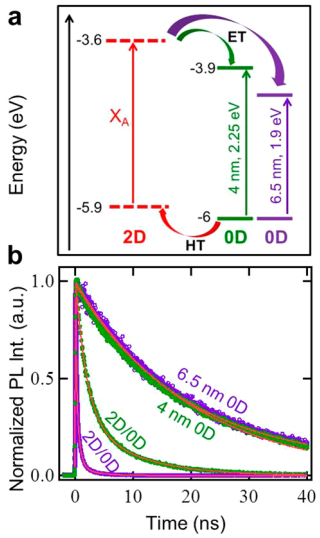

Figure 2. Electron transfer (ET) vs hole transfer (HT) at the 2D/0D interface. (a) Energy band alignment for 2D-WS_2 monolayer and 0D-QDs of different sizes; the 4 nm CdSe core diameter particles has the PL at 2.25 eV and the 6.5 nm CdSe core diameter has PL at 1.9 eV. The VBM and CBM values for the non-interacting 0D-QDs and the 2D-WS_2 semiconductor are taken from previous reports, refs 21 and 22, respectively. The thick arrows indicate that HT driving force is the same for both 0D-QD sizes, but the driving force for ET is greater in the case of 6.5 nm-diameter 0D-QD. The values of VBMs and CBMs are estimated based on previous reports.[13,21] (b) Decay of the peak PL intensities for the two 0D-QDs measured outside and inside the 2D-WS_2 crystal, as indicated 0D and 2D/0D, respectively. The PL was monitored around the QDs emission peaks. Solid red lines are fits to a single-exponential decay function in the case of 0D and to a biexponential decay function in the case of 2D/0D.

DOI: 10.1021/jacs.6b08883
J. Am. Chem. Soc. 2016, 138, 14713−14719

Ultrafast Dynamics of Electron Transfer and Formation of Hybrid Excitons. After ruling out the possibility of energy transfer and concluding that electron transfer from the 2D-WS_2 monolayers to 0D-QDs is the dominant charge-transfer pathway, we carried out femtosecond transient absorption (TA) measurements to confirm the electron-transfer process and measure its time-scale (see methods section in the Supporting Information). One way to do that is to exclusively excite the 2D-WS_2 crystal in the heterostructure and probe the 0D-QD lowest exciton transition. Before proceeding with that, and in order to have a reference TA data of 0D-QDs, we first carried out TA experiments for the 0D-QD (4 nm size) with 2.5 eV excitation, which is sufficient to excite the 0D-QD lowest exciton 1S and higher excitons as shown in Figure 3a,b. The negative signal observed around the

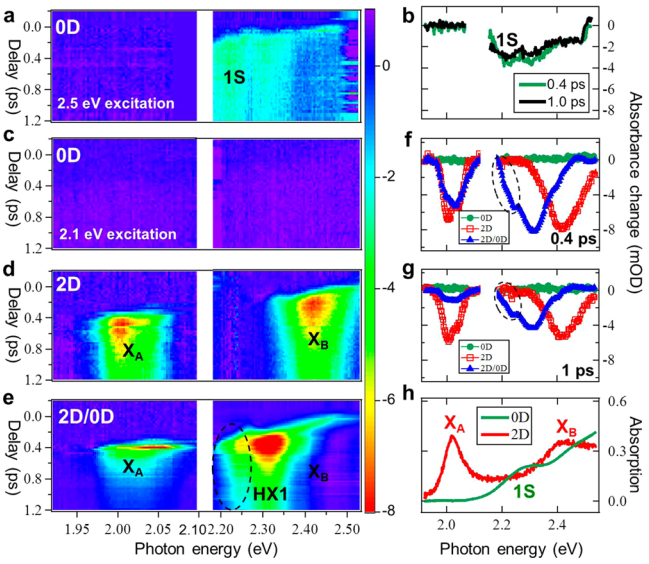

Figure 3. Transient absorption measurements. (a) TA time−energy map for the 0D-QDs on an SiO_2/Si substrate following excitation at 2.5 eV. (b) Cuts from (a) at 400 fs and 1 ps as indicated. (c) TA time−energy map for the 0D-QDs on SiO_2/Si substrate following excitation at 2.1 eV. No noticeable signal was observed. (d) TA for a 2D-WS_2 crystal on SiO_2/Si substrate without the 0D-QDs following excitation at 2.1 eV, showing depletion of band-edge excitons 2D-X_A and 2D-X_B. (e) TA for the same 2D-WS_2 crystal but covered with 0D-QDs on SiO_2/Si substrate following excitation at 2.1 eV, showing depletion of the 0D-QD 1S (highlighted with the dashed ellipse), quenching of 2D-X_A and 2D-X_B depletions, and formation of HX1 depletion. The color bar for panels a, c, d, and e indicates the absorbance change in mOD. The delayed signal at lower photon energies is due to the temporal chirp of the spectrally broad probe while passing through an 800 nm filter and a dichroic filter (800-F and DF in Figure S2). (f) Cuts from (c), (d), and (e) at 400 fs time-delay, as indicated. (g) Same as (f) but at 1 ps time-delay. The data around 2.1 eV are omitted due to zero-probe intensity resulting from the dichroic filter used in the experiment. (h) Steady-state absorption spectra for the isolated 0D-QDs and 2D-WS_2 monolayer on a quartz substrate.

1S exciton is not due only to the depletion of the 1S exciton but, it also includes stimulated emission, which usually appears to the "red" side of the exciton depletion. Additionally, due to the possibility of multiple excitons generation,[9] at early time delays, many-body interactions may cause shifts and broadening in exciton absorption.[9] Consequently, in order to estimate the 0D-QDs exciton binding energy, it is suitable to consider the steady-state absorption, which gives ∼180−190 meV. This value is comparable to reported calculations.[26]

Based on the UV−vis absorption spectrum of 0D-QDs, the 1S lowest exciton is located at ∼2.25 eV; therefore, an excitation at 2.1 eV in TA experiment is insufficient for direct excitation of 0D-QDs. Indeed, Figure 3c shows that excitation of the 0D-QDs located outside the 2D-WS_2 crystal on the SiO_2/Si substrate did not generate any noticeable transient signal. In the case of a 2D-WS_2 monolayer without 0D-QDs, the TA signals shown in Figure 3d were found to contain 2D-X_A (∼2 eV) and 2D-X_B (∼2.4 eV) exciton depletions. Although the excitation energy is below the 2D-X_B exciton, the 2D-X_B depletion can be formed based on the state-filing effect where upon absorption of 2.1 eV photons, electrons from deeper levels in the VB can move up to the VBM to fill-up the hole of 2D-X_A,[13,14,19] which depletes the ground state of the 2D-X_B exciton. In the case of the hybrid system, in addition to the 2D-X_A and X_B exciton depletions, TA traces shown in Figure 3e contain an additional depletion band around ∼2.25 eV corresponding to the 0D-QD 1S lowest exciton. Noting that, shown in Figure 3f,g are transient spectra of 0D-QDs, 2D-WS_2, and the hybrid sample at 400 fs and 1 ps, respectively. Since 2.1 eV photons are insufficient for 0D-QD excitation (see Figure 3h), this depletion can form as a consequence of the following: (1) energy transfer from the excited 2D-WS_2 to the 0D-QDs, (2) hole transfer from the 2D-VBM to the 0D-VBM, or (3) electron transfer from the 2D-CBM to the 0D-CBM. Because the 0D-QD bandgap (∼2.25 eV) is greater than that of the 2D-WS_2 (∼2 eV), energy transfer from the 2D-WS_2 monolayer to the 0D-QD is excluded, and hole transfer from the 2D-WS_2 VBM to 0D-QDs is excluded as well based on the band energy alignment shown in Figure 1c, where the 0D-VBM is lower than the 2D-VBM. Also, although hole transfer from deeper levels in the 2D-WS_2 VB to the 0D-QD VB is possible, these hole-transfer channels are not the dominant charge-transfer pathway, since the markedly dissimilar PL decays measured in Figure 2b should have been similar in this case for both QD sizes since, as discussed in the previous section, due to similar driving forces for hole transfer to 0D-QD of different sizes (see Figure 2a) resulting from the VBM insensitivity to the size of the 0D-QD.[21] Consequently, it is most likely that electron transfer from the 2D-WS_2 to the 0D-QD is more responsible for the observed depletion of the 0D-QD 1S exciton.

A close examination of the TA spectra shown in Figures 3e−g suggests that, in the case of the 2D/0D heterostructure, in addition to the 1S and the 2D exciton depletions, a new depletion band forms between the 0D-1S and 2D-X_B excitons. Because the delayed formation of this new absorption band accompanies the disappearance of the 2D-X_B, in addition to the fact that this band is stronger and appears to the "blue" side of the 1S depletion, it is likely that this band reflects the formation of a HX resulting from the electron transfer to the 0D-QD. We note that we corrected for the temporal chirp in the white light probe (see Figures S2 and S3 in the Supporting Information). Based on its absorption location, this HX1 forms between the transferred electron, now located at the QD's CBM, and the 2D-X_B hole left in the 2D VB.

We note that TA measurements for the 6.5 nm core size QDs interfaced with the 2D-WS_2 crystal are challenging since a selective excitation of the 2D-WS_2 monolayer is not possible. In fact, an excitation of the heterostructure at 2.1 eV would excite the 6.5 nm core-size QD as well, and consequently, the resulting depletion of the 1S exciton will not provide

DOI: 10.1021/jacs.6b08883
J. Am. Chem. Soc. 2016, 138, 14713−14719

information about the charge transfer from the 2D-WS_2 semiconductor.

Steady-State Absorption and Binding Energy of Hybrid Excitons. To confirm the formation of HXs, we carried out steady-state absorption measurements for the 0D-QDs (4 nm size), the 2D-WS_2 crystal, and the same 2D-WS_2 crystal covered with 0D-QDs. The spectra are shown in Figure 4a. Note that the measurements were carried out on a quartz substrate, and absorption was derived as follows: First we measured the light transmitted through the 2D-WS_2 crystal covered with 0D-QDs—this was taken as T_{on}. Next we moved just outside the perimeter of the 2D-WS_2 crystal and measured the light transmitted through the quartz substrate covered with 0D-QDs—this was taken as T_{off}. Then, the absorbance, A, was calculated as $-\log_{10}(T_{on}/T_{off})$; doing it this way made the quartz substrate *plus* 0D-QDs a reference. For 2D-WS_2 and 0D-QDs spectra, the absorbance is obtained the same way, but the bare quartz substrate is the reference. To obtain the net effect of the presence of 0D-QDs on the 2D-WS_2 crystal, the absorbance spectrum of 2D-WS_2 was subtracted from that of 2D/0D, and the resulting spectrum is plotted as in Figure 4b. We also carried out similar measurements on three additional crystals as shown in Figure S3. This difference spectra for all the studied samples contain two extrema oriented oppositely near the 2D-X_A exciton (~2 eV), which are due to the shift of the 2D-X_A exciton in the presence of the 0D-QDs that causes a change in the dielectric environment. At higher photon energies, around the 2D-X_B exciton (~2.43 eV), the difference spectra contain two distinct absorption bands; HX1 at ~2.3 eV and HX2 at ~2.7 eV. Because HX1 is similar to that observed in transient data shown in Figure 3e, which resulted from electron transfer to the 0D-QD, it is likely that HX1 and HX2 reflect the formation of hybrid excitons (noting that HX2 is out of the detection range in TA measurements). In this case, based on the spectral positions of HX1 and HX2, the holes of HX1 and HX2 are those of 2D-X_B exciton and higher excitons such as 2D-X_C, respectively as depicted in Figure 4c. Interestingly, the energy difference between HX1 and 2D-X_A (~400 meV) is comparable to the spin−orbit split in the VB of the 2D-WS_2 monolayer,[19,27] which confirms that the hole of HX1 is that of 2D-X_B exciton. Regarding HX2, its assignment is not trivial because while 2D-X_A and X_B excitonic transitions are well known,[19,27,28] it is until recently that the 2D-X_C transition was assigned to arise between levels where the VB and CB are "nested" in the Brillouin zone.[28] Interestingly, the estimated energy distance between HX1 and HX2 (~400 meV) is similar to that between the 2D-X_B VBM and the lower energy end of the "nesting" region in the VB where the 2D-X_C transition takes place. Consequently, it is likely that HX2 forms between the 2D-X_C hole in the 2D-WS_2 and the electron in the 0D-QD CBM as depicted in Figure 4c.

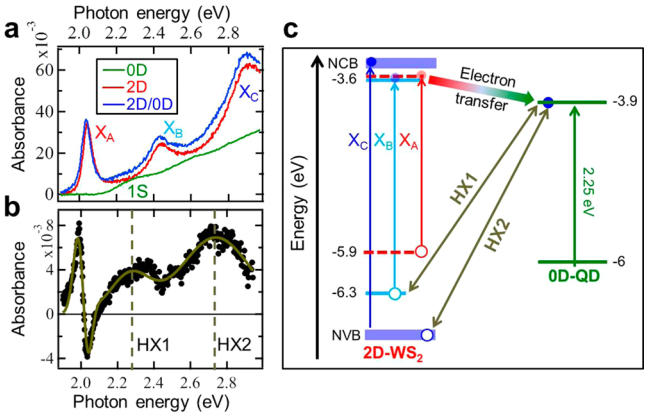

Figure 4. Formation of hybrid excitons (HXs). (a) Measured absorption spectra of 0D-QDs of 4 nm diameter (multiplied by a factor of 3), 2D-WS_2 monolayer, and 2D/0D heterostructure as indicated. The spectrum of the 2D/0D hybrid is obtained by measuring the transmission on and off the 2D/0D heterostructure in a sample that is all covered with 0D-QDs (0D-QDs are on and off the 2D-WS_2 crystal); consequently, the contribution of 0D-QDs absorption to the spectrum of 2D/0D, calculated as $-\log_{10}(T_{on}/T_{off})$, is canceled out. All the measurements are carried out on a quartz substrate. (b) Difference absorbance spectrum obtained after subtraction of the 2D spectrum from that of 2D/0D shown in (a). The thick solid line is a guide for the eye, and the vertical dashed lines indicate the centers of HX1 and HX2. (c) Energy band alignment of the 2D-WS_2 monolayer and the 4 nm 0D-QD. The VBM and CBM values for the non-interacting 0D-QDs and the 2D-WS_2 semiconductor are taken from previous reports, refs 21 and 22, respectively. Also shown are the VBM of the 2D-X_B exciton which is lower than the VBM of 2D-X_A exciton by ~400 meV,[19] and the 2D-X_C transition which happens between the "nesting" bands in the VB (NVB) and in the CB (NCB).[28] The formation of HX1and HX2 hybrid excitons is indicated by the double-sided arrows.

Based on the VBM and CBM values for 0D-QDs and the 2D-WS_2 semiconductor,[21,22] HX1 is expected to be at ~2.4 eV (Figure 4c), but according to Figure 4b, the HX1 absorption peak was observed at ~2.26 eV. This difference of ~140 meV corresponds to the binding energy of HX1, which indicates that it is more weakly bound than excitons in 2D-WS_2 monolayers, which have a binding energy ranging from 300 to 700 meV according to different reports.[8,29]

Although it is possible to form a HX between the hole of the 2D-X_A exciton and the electron transferred to the QD's CBM, our results did not suggest that. This is likely because upon creation of 2D-X_A excitons followed by electron transfer to the 0D-QD, electrons at deeper energy levels in the 2D VB can move up and fill-up the remaining 2D-X_A hole. In fact, according to Figure 5a, the 2D-X_A exciton transition did not remain depleted after electron transfer to the 0D-QD. Instead, its depletion signal decayed indicating that electrons from deeper levels compensated the hole. Furthermore, no evidence was found for other HXs that might have resulted as a consequence of hole transfer from the 2D-WS_2 to the 0D-QDs, supporting the argument that hole transfer was not the dominant charge-transfer channel, in agreement with the PL lifetime measurements discussed above in Figure 2.

Electron-Transfer Time-Scale. To extract the electron transfer and HX1 formation time-scale, we carried out TA measurements at early time-delays (<2 ps) with fine steps (5 fs) and higher number of averaged laser shots at each delay (2000 absorbance changes are averaged at each time-step). First, we corrected for the temporal chirp in the white light continuum probe (see Figure S3 and the corresponding text in the Supporting Information), and then we measured the depletion dynamics of 2D-X_A and 0D-QD 1S as shown in Figure 5a,b, respectively. We not that early time-delay dynamics (<350 fs) are shown in Figure 5c,d. These dynamics are well-described by a biexponential function, and the parameters of the converged fits are listed in Tables S2−S4. In the case of 2D-WS_2 sample without the 0D-QDs, the 2D-X_A exciton depletion measured at ~2 eV following the nearly resonant excitation at 2.1 eV decays with 0.9 and 12.6 ps time constants, which describe the non-

DOI: 10.1021/jacs.6b08883
J. Am. Chem. Soc. 2016, 138, 14713−14719

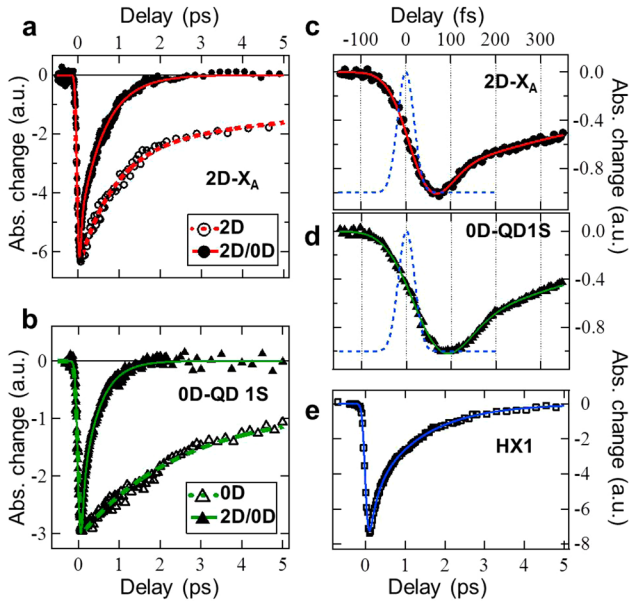

Figure 5. Electron-transfer time at the 2D/0D interface. (a) 2D-X_A exciton depletion dynamics in the absence (open circles) and in the presence of 0D-QDs (filled circles) following excitation at 2.1 eV. Solid and dashed lines are biexponential fits. (b) 0D-QD 1S exciton depletion dynamics in the absence of 2D-WS_2 monolayer excited at 2.5 eV (open triangles) and in the presence of 2D-WS_2 monolayer excited at 2.1 eV (filled triangles). Solid and dashed lines are biexponential fits. (c) Early time-delay dynamics of 2D-X_A exciton depletion measured at the 2D/0D interface and fit as shown in (a). The dashed line is the ~45 fs excitation laser pulse. (d) Early time-delay dynamics of 0D-QD 1S exciton depletion measured upon 2.1 eV excitation of the 2D/0D interface and fit as shown in (b). Since 2.1 eV photons are insufficient for exciting the 0D-QD 1S transition, its depletion is a consequence of electron transfer from the 2D-WS_2 CBM. (e) Depletion formation and decay dynamics of HX1 measured upon excitation of the 2D/0D nanocomposite (open squares) fit to a biexponential decay function (solid plot).

radiative recombination through Auger-type scattering and defect-assisted relaxations, and the radiative electron−hole recombination,[30,31] respectively. In the presence of 0D-QDs, however, more than 75% of the depletion signal decays with a time constant of ~18 fs, and the remaining ~25% decays with ~0.62 ps time constant. Similar quenching results for the 2D-X_B exciton depletion dynamics are shown in Figure S5 and Table S2. For 0D-QD 1S exciton depletion decay following excitation at 2.5 eV (sufficient for 0D-QD excitation) of the 0D-QDs without the 2D-WS_2 monolayer, the time constants went from 16 and 417 ps to 34 and 416 fs, respectively, when the 2D/0D interface was excited at 2.1 eV (see Table S3). Since the 2.1 eV photons were nearly resonant with the 2D-X_A transition, the depletion formation of the 2D-X_A exciton should be instantaneous and determined by the laser pulse duration. Because the 2.1 eV photons are not sufficient for 0D-QDs excitation as demonstrated in Figure 3c, the 0D-QD 1S exciton depletion formation observed in the case of 2D/0D sample reflects the electron-transfer time from the 2D-WS_2 CBM to the 0D-QD CBM. In order to extract this ultrashort time, the depletion formations and decays of 2D-X_A and 0D-QD 1S excitons were fit by convoluting a biexponential decay function with a Gaussian instrument response function (IRF) with 45 fs duration. In the case of the 2D-X_A depletion, the dynamics were fit using an IRF having duration equal to that of the laser pulse (45 fs). In the case of 0D-QD 1S depletion, the converged fit returned ~57 fs as depletion formation time, indicating that the 12 fs difference reflects the electron-transfer time from the 2D-WS_2 CBM to 0D-QDs. But, since this value is much smaller than the pulse duration (~45 fs), one can only conclude that the electron-transfer time is on the sub-45 fs time-scale.

The fitting of HX1 depletion dynamics shown in Figure 5e to a biexponential decay function returned two time constants: 19 fs and 1.3 ps. The complete fitting parameters are provided in Table S4. This decay of the signal does not necessarily indicate radiative recombination of the electron located in the 0D-QD and the hole left in the 2D-WS_2 monolayer. In fact, such ultrashort decay times are typically more characteristic of non-radiative decay through Auger scattering or charge trapping at defects.[30,31] Additionally, based on the relatively low binding energy (~140 meV) of HX1, dissociation of this IX is possible, which would also lead to a decay of its depletion signal. However, if HX1 dissociates, the 0D-QD 1S transition would be expected to remain depleted until the electron in the CBM of the 0D-QD relaxes. Since the 1S depletion signal shown in Figure 5b decays concurrently with that of 2D-X_A in Figure 5a and the fast component of HX1, we conclude that electron and/or hole trapping is most likely the reason for the majority of the HX1 depletion decay observed in Figure 5e.

The sub-45 fs electron-transfer time may seem surprisingly short, considering that the electron needs to tunnel through a thick barrier formed of ZnS shell and octadecylamine capping ligand that separate the 2D and 0D structures. Considering that the charge-transfer rate k_{CT} is directly related to the barrier potential $V(z)$ through the following equation,

$$k_{CT} \sim \exp\left[-\int \sqrt{\frac{2mV(z)}{\hbar}}\, dz\right]$$

where m is the effective mass of the charge,[32] one can engineer different 0D-QD shells and capping ligands to control the efficiency of the charge-transfer process. For example, it has been reported that in the case of PbSe QDs treated with hydrazine or 1,2-ethanedithiol, capping was found to enhance the electronic coupling with single-crystalline (110) TiO_2, and accelerate the electron-transfer process to a sub-50 fs time-scale.[33]

CONCLUSIONS

In summary, dynamic ultrafast spectroscopic pump−probe measurements indicate that following selective photoexcitation of a 2D-WS_2 monolayer, predominantly electron transfer occurs to deplete the CdSe/ZnS core/shell QDs lowest exciton on a sub-45 fs time-scale, resulting in the formation of HX corresponding to electrons located in the QDs and holes located in the 2D-WS_2 crystal. This HX is revealed by the appearance of a new absorption band centered at 2.26 eV during the first ~1 ps after excitation, during which time the 2D-X_B exciton depletion is decayed. Although hole transfer is not excluded, we conclude that electron transfer from the 2D excitons to the 0D-QD is the dominant charge-transfer pathway on the basis of photoluminescence lifetime measurements using different 0D-QD sizes. Although the HX measured in this study was short-lived, improvements in 2D crystal quality synthesized by CVD and choice of capping ligand and shell of 0D-QDs may be envisioned to extend further the lifetime of indirect HXs, and consequently allowing efficient collection of charges in 0D/2D heterostructures-based optoelectronic devices. The demon-

DOI: 10.1021/jacs.6b08883
J. Am. Chem. Soc. 2016, 138, 14713−14719

stration of such 0D/2D HXs between 2D and 0D materials offers a wide range of opportunities to design hybrid heterostructures for various optoelectronic, catalytic, and sensing applications due to the variety of QDs and size-tunability of their band gaps.

■ ASSOCIATED CONTENT

Supporting Information

The Supporting Information is available free of charge on the ACS Publications website at DOI: 10.1021/jacs.6b08883.

Description of sample preparation and characterization using ultrafast spectroscopy, steady-state absorption, photoluminescence, and morphological characterization using TEM; Tables S1−S4 listing the parameters of the converged fits of ultrafast exciton and charge-transfer dynamics (PDF)

■ AUTHOR INFORMATION

Corresponding Author

*boulesbaaa@ornl.gov

Notes

The authors declare no competing financial interest.

■ ACKNOWLEDGMENTS

This research was conducted at the Center for Nanophase Materials Sciences, which is a DOE Office of Science User Facility. Synthesis of the two-dimensional materials was supported by the Materials Science and Engineering Division, Office of Basic Energy Sciences, U.S. Department of Energy.

■ REFERENCES

(1) Bernardi, M.; Palummo, M.; Grossman, J. C. *Nano Lett.* **2013**, *13*, 3664−3670.
(2) Mak, K. F.; Lee, C.; Hone, J.; Shan, J.; Heinz, T. F. *Phys. Rev. Lett.* **2010**, *105*, 136805.
(3) Ross, J. S.; Wu, S.; Yu, H.; Ghimire, N. J.; Jones, A. M.; Aivazian, G.; Yan, J.; Mandrus, D. G.; Xiao, D.; Yao, W.; Xu, X. *Nat. Commun.* **2013**, *4*, 1474.
(4) Mak, K. F.; Shan, J. *Nat. Photonics* **2016**, *10*, 216−226.
(5) Tsai, M. L.; Su, S. H.; Chang, J. K.; Tsai, D. S.; Chen, C. H.; Wu, C.; Li, L. J.; Chen, L. J.; He, J. H. *ACS Nano* **2014**, *8*, 8317−8322.
(6) Gan, L. Y.; Zhang, Q.; Cheng, Y.; Schwingenschlögl, U. *J. Phys. Chem. Lett.* **2014**, *5*, 1445−1449.
(7) Kuc, A.; Zibouche, N.; Heine, T. *Phys. Rev. B: Condens. Matter Mater. Phys.* **2011**, *83*, 245213.
(8) Chernikov, A.; Berkelbach, T. C.; Hill, H. M.; Rigosi, A.; Li, Y.; Aslan, O. B.; Reichman, D. R.; Hybertsen, M. S.; Heinz, T. F. *Phys. Rev. Lett.* **2014**, *113*, 076802.
(9) Klimov, V. I. *Annu. Rev. Phys. Chem.* **2007**, *58*, 635−673.
(10) Prins, F.; Goodman, A. J.; Tisdale, W. A. *Nano Lett.* **2014**, *14*, 6087−6091.
(11) Prasai, D.; Klots, A. R.; Newaz, A.; Niezgoda, J. S.; Orfield, N. J.; Escobar, C. A.; Wynn, A.; Efimov, A.; Jennings, G. K.; Rosenthal, S. J.; Bolotin, K. I. *Nano Lett.* **2015**, *15*, 4374−4380.
(12) Raja, A.; Montoya-Castillo, A.; Zultak, J.; Zhang, X. X.; Ye, Z.; Roquelet, C.; Chenet, A. A.; van der Zande, A. M.; Huang, P.; Jockusch, S.; Hone, J.; Reichman, D. R.; Brus, L. E.; Heinz, T. F. *Nano Lett.* **2016**, *16*, 2328−2333.
(13) Hong, X.; Kim, J.; Shi, S. F.; Zhang, Y.; Jin, C.; Sun, Y.; Tongay, S.; Wu, J.; Zhang, Y.; Wang, F. *Nat. Nanotechnol.* **2014**, *9*, 682−686.
(14) Ceballos, F.; Bellus, M. Z.; Chiu, H. Y.; Zhao, H. *ACS Nano* **2014**, *8*, 12717−12724.
(15) Fang, H.; Battaglia, C.; Carraro, C.; Nemsak, S.; Ozdol, B.; Kang, J. S.; Bechtel, H. A.; Desai, Si. B.; Kronast, F.; Unal, A. A.; Conti, G.; Conlon, C.; Palsson, G. K.; Martin, M. C.; Minor, A. M.; Fadley, C. S.; Yablonovitch, E.; Maboudian, R.; Javey, A. *Proc. Natl. Acad. Sci. U. S. A.* **2014**, *111*, 6198−6202.
(16) Rivera, P.; Schaibley, J. R.; Jones, A. M.; Ross, J. S.; Wu, S.; Aivazian, G.; Klement, P.; Seyler, K.; Clark, G.; Ghimire, N. J.; Yan, J.; Mandrus, D. G.; Yao, W.; Xu, X. *Nat. Commun.* **2015**, *6*, 6242.
(17) Gong, Y.; Lin, J.; Wang, X.; Shi, G.; Lei, S.; Lin, Z.; Zou, X.; Ye, G.; Vajtai, R.; Yakobson, B. I.; Terrones, H.; Terrones, M.; Tay, B. K.; Lou, J.; Pantelides, S. T.; Liu, Z.; Zhou, W.; Ajayan, P. M. *Nat. Mater.* **2014**, *13*, 1135−1142.
(18) Zhu, X.; Monahan, N. R.; Gong, Z.; Zhu, H.; Williams, K. W.; Nelson, C. A. *J. Am. Chem. Soc.* **2015**, *137*, 8313−8320.
(19) Boulesbaa, A.; Huang, B.; Wang, K.; Lin, M. W.; Mahjouri-Samani, M.; Rouleau, M.; Xiao, K.; Yoon, M.; Sumpter, B.; Puretzky, A.; Geohegan, B. *Phys. Rev. B: Condens. Matter Mater. Phys.* **2015**, *92*, 115443.
(20) Zhang, Y.; Jing, P.; Zeng, Q.; Sun, Y.; Su, H.; Wang, Y. A.; Kong, X.; Zhao, J.; Zhang, H. *J. Phys. Chem. C* **2009**, *113*, 1886−1890.
(21) Tvrdy, K.; Frantsuzov, P. A.; Kamat, P. V. *Proc. Natl. Acad. Sci. U. S. A.* **2011**, *108*, 29−34.
(22) Gong, C.; Zhang, H.; Wang, W.; Colombo, L.; Wallace, R. M.; Cho, K. *Appl. Phys. Lett.* **2013**, *103*, 053513.
(23) Kozawa, D.; Carvalho, A.; Verzhbitskiy, I.; Giustiniano, F.; Miyauchi, Y.; Mouri, S.; Castro Neto, A. H.; Matsuda, K.; Eda, G. *Nano Lett.* **2016**, *16*, 4087−4093.
(24) Broser, I.; et al. Landolt−Börnstein New Series Group III. *Physics of II−VI and I−VII Compounds, Semimagnetic Semiconductors*; Condensed Matter 17b; Madelung, O., Ed.; Springer: New York, 1982.
(25) Zheng, K.; Žídek, K.; Abdellah, M.; Zhang, W.; Chábera, P.; Lenngren, N.; Yartsev, A.; Pullerits, T. *J. Phys. Chem. C* **2014**, *118*, 18462−18471.
(26) Elward, J. M.; Chakraborty, A. *J. Chem. Theory Comput.* **2013**, *9*, 4351−4359.
(27) Mai, C.; Semenov, Y. G.; Barrette, A.; Yu, Y.; Jin, Z.; Cao, L.; Kim, K. W.; Gundogdu, K. *Phys. Rev. B: Condens. Matter Mater. Phys.* **2014**, *90*, 041414.
(28) Kozawa, D.; Kumar, R.; Carvalho, A.; Amara, K. K.; Zhao, W.; Wang, S.; Toh, M.; Ribeiro, R. M.; Castro Neto, A. H.; Matsuda, K.; Eda, G. *Nat. Commun.* **2014**, *5*, 4543.
(29) Ye, Z.; Cao, T.; O'Brien, K.; Zhu, H.; Yin, X.; Wang, Y.; Louie, S. G.; Zhang, X. *Nature* **2014**, *513*, 214−218.
(30) Moody, G.; Schaibley, J.; Xu, X. *J. Opt. Soc. Am. B* **2016**, *33*, c39−c49.
(31) Wang, H.; Zhang, C.; Rana, F. *Nano Lett.* **2015**, *15*, 339−345.
(32) Chen, C. Y.; Cheng, C. T.; Yu, J. K.; Pu, S. C.; Cheng, Y. M.; Chou, P. T.; Chou, Y. H.; Chiu, H. T. *J. Phys. Chem. B* **2004**, *108*, 10687−10691.
(33) Tisdale, W. A.; Williams, K. J.; Timp, B. A.; Norris, D. J.; Aydil, E. S.; Zhu, X. Y. *Science* **2010**, *328*, 1543−1547.

DOI: 10.1021/jacs.6b08883
J. Am. Chem. Soc. 2016, 138, 14713−14719